Flat-field correction technique for digital detectors

Seibert, James, Boone, John, Lindfors, Karen

James Anthony Seibert, John M. Boone, Karen K. Lindfors, "Flat-field correction technique for digital detectors," Proc. SPIE 3336, Medical Imaging 1998: Physics of Medical Imaging, (24 July 1998); doi: 10.1117/12.317034

SPIE.

Event: Medical Imaging '98, 1998, San Diego, CA, United States

Flat-field correction technique for digital detectors

J. Anthony Seibert, John M. Boone, and Karen K. Lindfors
Department of Radiology[1], University of California Davis Medical Center
Sacramento, CA 95817

ABSTRACT

The effects of the stationary noise patterns and variable pixel responses that commonly occur with uniform exposure of digital detectors can be effectively reduced by simple "flat-field" image processing methods. These methods are based upon a linear system response and the acquisition of an image (or images) acquired at a high exposure to create an inverse matrix of values that when applied to an uncorrected image, remove the effects of the stationary noise components. System performance is optimized when the correction image is totally free of statistical variations. However, the stationary noise patterns will not be effectively removed for flat-field images that are acquired at a relatively low exposure or for systems with non-linear response to incident exposure variations. A reduction in image quality occurs with the incomplete removal of the stationary noise patterns, resulting in a loss of detective quantum efficiency of the system. A more flexible approach to the global flat-field correction methodology is investigated using a pixel by pixel least squares fit to "synthesize" a variable flat-field image based upon the pixel value (incident exposure) of the image to be corrected. All of the information is stored in two "equivalent images" containing the slope and intercept parameters. The methodology provides an improvement in the detective quantum efficiency (DQE) due to the greater immunity of the stationary noise variation encoded in the slope/intercept parameters calculated on a pixel by pixel basis over a range of incident exposures. When the raw image contains a wide range of incident exposures (e.g., transmission through an object) the variable exposure flat-field correction methodology proposed here provides an improved match to the fixed-point noise superimposed in the uncorrected image, particularly for the higher spatial frequencies in the image as demonstrated by DQE(f) measurements. Successful application to clinical digital mammography biopsy images has been demonstrated, and benefit to other digital detectors appears likely.

Keywords: flat field correction, image optimization, image quality, noise power spectrum, detective quantum efficiency, digital detectors, digital mammography biopsy system

1. CONVENTIONAL FLAT-FIELD IMPLEMENTATION

Digital detectors are prone to several sources of stationary (fixed-point) noise sources, such as pixel dropouts in CCD or flat-panel arrays, "chicken-wire" artifacts arising from fiber-optic taper couplings, variable pixel gain, and artifacts due to misuse of the detector, among others. As this noise source is consistent from image to image, a uniform field image, I(x,y,t), is acquired at a typical exposure over a time period t that is clinically encountered. This image (or average of multiple images to reduce random uncertainty) is modified by subtracting the DC offset (black level) signal, B(x,y,t), accumulated over the exposure time, t, to produce the offset corrected image, $I_B(x,y)$ according to Eq. 1.

$$I_B(x,y) = I(x,y,t) - B(x,y,t) \qquad (1)$$

Note that the DC offset signal accumulates during the integration time, t, and must be matched to the exposure time of the image acquisition. The offset corrected image, $I_B(x,y)$ in Eq. 1, is then normalized by the average pixel value within the image array, $\langle I_B(x,y) \rangle$ and scaled by a constant integer value, S, to avoid integer truncation (Eq. 2). In practice, S is chosen according to the maximum value of the normalized array to avoid exceeding the 16 bit integer limit. The output value is the "normalized flat-field correction image", FF(x,y), and is typically stored as a two byte per pixel integer array. However, for the implementation described in this paper, the flat-field image is stored as a floating-point matrix in order to preserve precision of the fractional values of the correction matrix, with the constant S set equal to 1.

[1] Further author information –
JAS (Correspondence): Radiology Research, FOLB-II-E, 2421 45th St, Sacramento, CA 95817; Email: jaseibert@ucdavis.edu; Telephone: 916-734-0311; Fax: 916-734-0316
JMB: Email: jmboone@ucdavis.edu; Telephone: 916-734-3158

Part of the SPIE Conference on Physics of Medical Imaging • San Diego, California • February 1998
SPIE Vol. 3336 • 0277-786X/98/$10.00

$$FF(x,y) = \frac{\langle I_B(x,y) \rangle}{I_B(x,y)} \times S \qquad (2)$$

Flat-field correction of a raw image, $I_1(x,y,t)$, begins by first removing the DC offset signal by subtraction of a dark current image acquired at the same exposure time. Pixel by pixel multiplication with the correction image, FF(x,y), results in the output corrected image, $C_1(x,y)$, according to Eq. 3.

$$C_1(x,y) = \left(I_1(x,y,t) - B(x,y,t)\right) \times FF(x,y) \qquad (3)$$

Non-stochastic noise patterns are reduced or eliminated by the application of Eq. 3. However, when the flat-field correction image and the raw image are acquired with a widely different incident exposure or under different x-ray scatter conditions, the stationary noise pattern might not be entirely canceled. Under such conditions, a loss of detective quantum efficiency occurs in the corrected image due to the increase in noise attributed to the non-canceled stationary noise [1]. Therefore, in a clinical image in which a wide range of exposures are incident upon the detector due to the anatomy of the imaged object, the flat-field correction is less than optimal, chiefly due to the uncertainty of the noise processes in both the raw image and the flat-field image.

2. VARIABLE EXPOSURE FLAT-FIELD IMPLEMENTATION

A proposed alternative plan is to construct a normalized flat-field image based upon a linear least squares measurement, pixel by pixel, over a range of incident exposures expected in a clinical image. In the conventional flat-field technique, several images are averaged to achieve greater immunity from random quantum statistics at a given (usually high) exposure. An implementation of the proposed method is to acquire these images at several incident exposure levels. First, 8 or more identical uniform images are acquired at a given incident exposure, and averaged. A corresponding number of dark-offset images, matched to the exposure time, are also acquired and averaged. An offset-corrected image is obtained from the difference with pixel by pixel subtraction. For a specific beam energy, this is repeated for low, medium, and high input exposures (n = 5 exposure levels), distributed equally over the useful dynamic range of the digital detector. This set of images is denoted as a function of exposure, $E_n(x,y)$. Based upon the known exposure to pixel value linearity of the digital system, a linear least squares fit is performed as a function of pixel value on the data set for each (x,y) pixel location as:

$$\text{linfit}_{n=1\to5} \left\{ E_n(x,y) \right\} \text{ for each (x,y) pixel location in the set of } n \text{ exposure images} \qquad (4)$$

where the function *linfit*{}represents a linear least squares computer algorithm, producing a slope $E_S(x,y)$ and intercept $E_I(x,y)$ value. The dark-field images are manipulated in an identical fashion, producing a slope, $D_S(x,y,t)$, and intercept, $D_I(x,y,t)$ data matrix. In both $E_I(x,y)$ and $D_I(x,y,t)$, the intercept values are close to 0.

The normalized exposure *variable* flat-field correction matrix VFF(x,y) is then calculated as

$$VFF(x,y) = \frac{\langle E_{SL}(x,y) \rangle}{E_{SL}(x,y)} \times C \qquad (5)$$

where $\langle E_{SL}(x,y) \rangle$ is the average of all of the calculated slope values. The intercept variable is not included in Eq. 5, since all intercept values are equal to or close to zero as expected, after the dark (offset) image correction. For the implementation described in this paper, C=1 and VFF(x,y) is stored as a floating point matrix to preserve precision of the fractional values.

Correction of a raw image $I_1(x,y,t)$ then proceeds by subtracting the offset gain and applying the variable exposure flat-field matrix:

$$V_1(x,y) = \left(I_1(x,y,t) - [D_S(x,y,t) \times t + D_I(x,y,t)]\right) \times VFF(x,y) \qquad (6)$$

for an exposure time t. The value in the square brackets adjusts for the dark current accumulation during the exposure time of the acquired raw image. $V_1(x,y)$ represents the output corrected image using the variable flat-field technique.

In the event that the exposure response of the detector system is non-linear, this methodology can be modified to include any functional fit on a pixel by pixel basis, by simply expanding the parameters that accurately describe the response. For instance, a polynomial response could be implemented with the storage of the individual pixel parameters in a set of separate flat-field matrices for the parameters calculated as a function of pixel value. Reconstruction of the non-linear flat field matrix would be based upon the parameters and the pixel value of the raw image to be corrected.

3. METHODS

A. Image acquisitions

An objective comparison of the two flat-field correction implementations described in part 2 was accomplished by evaluating the noise properties and effects on the detective quantum efficiency of images acquired on a 50×50 mm field of view digital mammography biopsy system (Mammovision, Fischer Imaging Corporation, Denver, CO). This device uses a cooled 1024×1024 pixel CCD camera coupled to a 2:1 de-magnification fiberoptic taper coated with a rare-earth Gd_2O_2S phosphor of ~34 mg/cm^2 thickness. The resultant pixel size at the detector plane was approximately 50 μm. For all experiments, images were acquired "raw", without any image processing or corrections applied. A no-scatter geometry was employed by placing a uniform Lucite attenuation block of 4 cm thickness on the tube collimator of the biopsy device. In this configuration, the source to detector plane distance was 66 cm, and the exit surface of the Lucite phantom to the detector was 52 cm (essentially eliminating the effects of x-ray scatter). X-ray exposure as a function of mAs at 26 kVp and 100 mA was determined with a calibrated 15 cc ionization chamber and electrometer (Keithley 35050A, Cleveland, OH). The chamber was positioned 58 cm from the source. Exposure linearity and reproducibility were verified, and all subsequent image acquisitions were acquired without the ion chamber. The selected manual mAs and the mR/mAs calibration corrected for inverse square falloff of the photon intensity determined incident exposure to the detector. Beam quality was measured by half-value layer measurements with type 1100 aluminum sheets. An estimate of 45092 photons/mm^2/mR incident on the detector was determined from the methodology and tabular data of Boone [2,3] based upon the kVp, object thickness, half value layer, and geometric set-up parameters. Line spread function (LSF) measurements were made in the vertical and horizontal directions of the image matrix. This was accomplished by acquiring an image of a 10μm slit in contact with the detector, with the long axis slightly angled to the rows and columns of the image matrix, using methods described by Fujita [4]. The resultant LSF distribution was used to calculate the pre-sampled Modulation Transfer Function (MTF). A non-linear least square fit of the MTF(f) was obtained using commercially available curve-fitting software for input into the calculation of the Detective Quantum Efficiency (DQE) in Eq.7.

Eight uniform images were acquired at each of the following mAs settings: 20, 80, 160, 240, and 320, expressly for the purpose of the creation of a low-noise "averaged" image for the flat-fielding procedures. In addition, 4 "dark noise" images were acquired with time integration periods of 0.2, 0.8, 1.6, 2.4 and 3.2 seconds, respectively, corresponding to the exposure times of the x-ray images. Each dark noise image set was averaged and then subtracted from the corresponding x-ray image, resulting in "offset-corrected" x-ray images at the specific input exposures. For conventional flat-fielding, each of these images was manipulated according to Eq. 2 and stored as a floating point array of fractional values, FF(x,y). For variable exposure flat-fielding, all of the offset corrected x-ray images were fit using linear regression on a pixel by pixel basis, according to Eq. 4, resulting in a slope and intercept value for each pixel in the matrix. The normalized variable flat-field image, VFF(x,y) was then calculated according to Eq. 5. Additionally, the dark acquisition image set was also fit to a linear least squares algorithm providing $D_S(x,y)$ and $D_I(x,y)$ values, enabling the creation of an offset correction image on a pixel by pixel basis based upon the exposure time.

B. Noise analysis

Two raw x-ray images were acquired at 20, 40, 80, 120, 160, 200, 240, 280, 320, 360, and 400 mAs respectively, corresponding to an incident exposure range of ~2.7 to ~55 mR and an average digital number value of ~250 to ~3500. A conventional flat-field correction of one image at each mAs was accomplished per Eq. 3 with $FF_{320\ mAs}$, $FF_{160\ mAs}$ and $FF_{80\ mAs}$, corresponding to a respective incident input exposure of approximately 45, 22, and 11mR, respectively. The same images were also corrected using the variable flat-field method, VFF, per Eq. 6. The noise characteristics were obtained by noise power spectrum (NPS) measurements, utilizing a one-dimensional NPS algorithm and synthesis of a 40 pixel digital "slit" (in the vertical direction) over a horizontal trace length of a 128 pixel array. A central 512×512 subarray of the 1024×1024 image was chosen to enable the convolution smoothing of the low-frequency variations in the image outside of the evaluated data

points. A total of 88 non-overlapping realizations comprised the ensemble set of the NPS estimate for each image, measured as a function of the pixel value variance. Each NPS estimate was scaled by the slit length divided by the trace length [5]. The average digital number value, DN_{avg} of the image within the analyzed area was calculated for normalization of the NPS(f) estimate to $NPS_N(f)$ in terms of exposure variations. Other parameters calculated were the Noise Equivalent Quanta (NEQ (f)) and DQE(f) [5,6,7] as described in Eq. 7:

$$DQE(f) = \frac{SNR^2_{out}}{SNR^2_{in}} = \frac{NEQ(f)}{q} = \frac{MTF^2(f)}{NPS_N(f) \times q} = \frac{(DN_{avg})^2 \times MTF^2(f)}{NPS(f) \times q} \qquad (7)$$

where q is the estimated #photons/mm^2 for the image used to compute the NPS(f). Subtracted images were also analyzed in a similar manner to determine the "floor" of the NPS estimate, after correcting for the factor of 2 noise introduced by the subtraction process.

C. Data comparisons

DQE measurements for a subset of the flat-fielded raw images acquired with 20 mAs (2.8 mR), 160 mAs (22 mR), and 320 mAs (45 mR) were generated. The flat-field correction matrices used were the variable flat-field correction, VFF, a conventional flat-field correction with an image produced from a 320 mAs (45 mR) acquisition of eight images, FF_{320}, and a correction image produced from an 80 mAs (12 mR) acquisition of eight images, FF_{80}. The total complement of raw images were also corrected (20 mAs plus 40 to 400 mAs images in steps of 40 mAs) with each flat-field matrix. DQE values at 2.5, 5.0 and 7.5 lp/mm were determined as a function of mAs (incident exposure to the detector).

4. RESULTS / DISCUSSION

The mAs linearity response of the x-ray system and the digital number value (ADU) to incident exposure of the digital imaging system are plotted in Figure 1, with the measurements and the best fit line illustrated. In each fit, the correlation coefficient, r^2 exceeded 0.999.

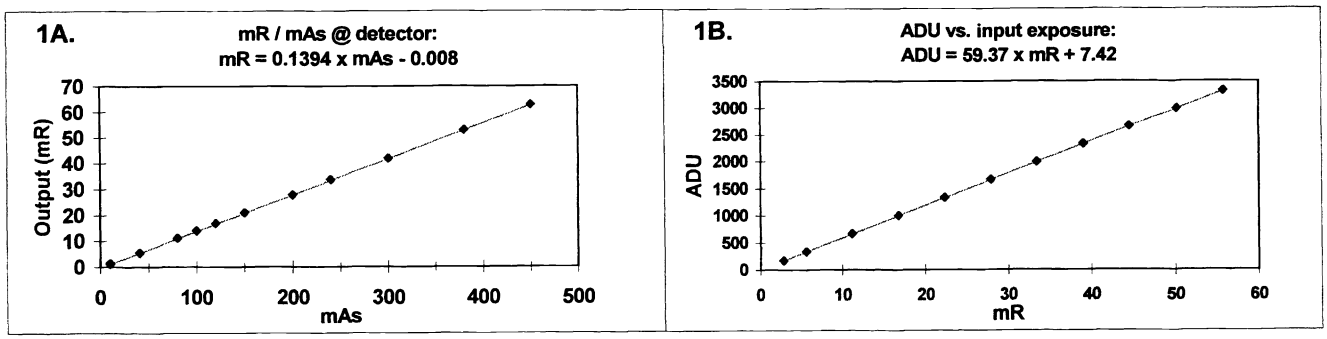

Figure 1. A. The mAs linearity of the x-ray generator is illustrated. B. The relationship of the incident exposure to the digital number (ADU) average value in the "offset-corrected" images is shown.

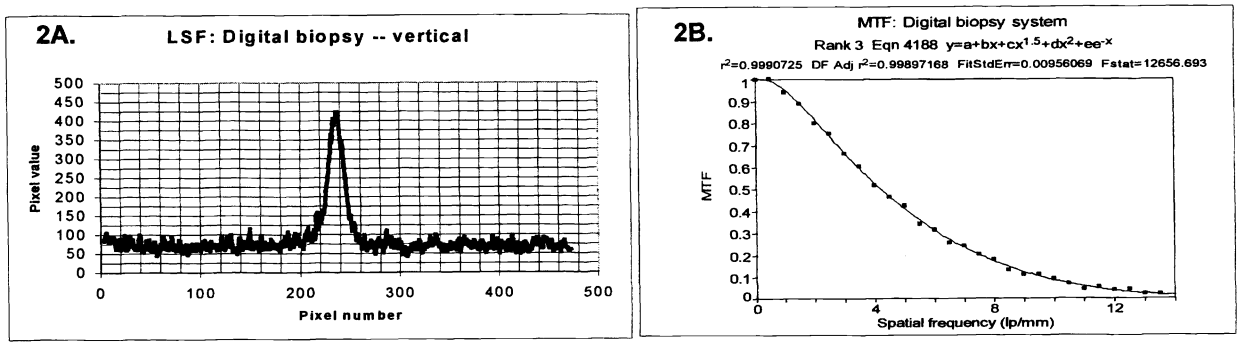

Figure 2. A. The LSF in the horizontal direction is illustrated. B. The corresponding pre-sampled MTF data points and fit to an analytic function is shown on the right. A 50 μm pixel size at the detector surface resulted in a Nyquist frequency of 10 lp/mm. Measurements in the vertical direction (not shown) resulted in a nearly identical MTF.

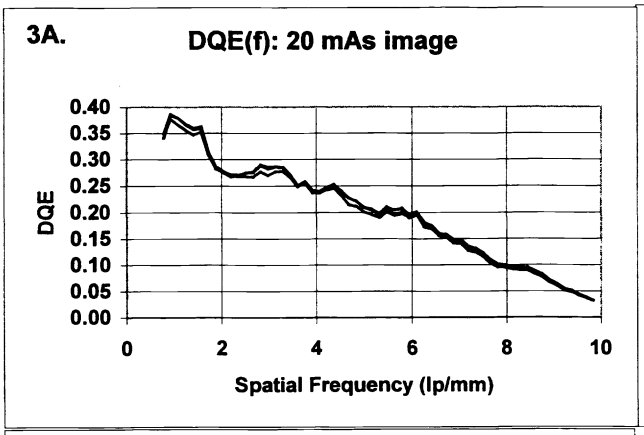

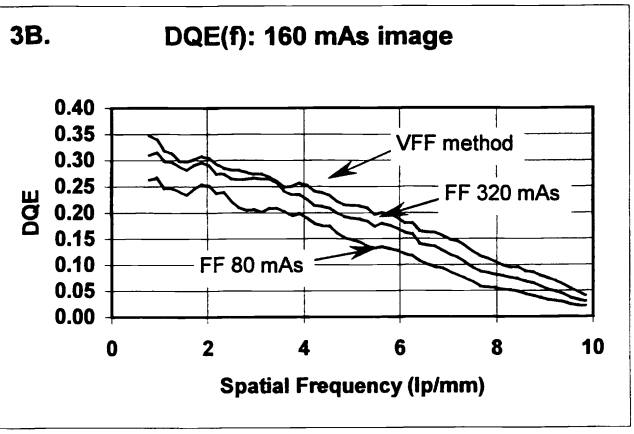

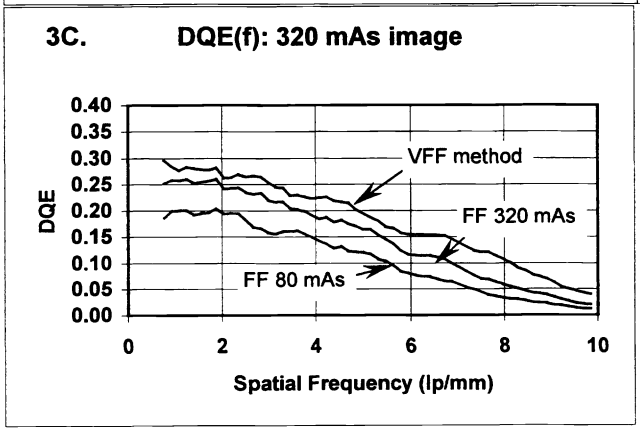

Figure 3. DQE(f) data for flat-field corrected raw images are illustrated.. A. Raw image acquired at 20 mAs (2.7 mR). B. Raw image acquired at 160 mAs (22 mR). C. Raw image acquired at 320 mAs (44 mR). In each, three separate lines appear, corresponding to the variable flat-field method (always the top curve), the FF_{320} correction (always the middle curve), and the FF_{80} curve.

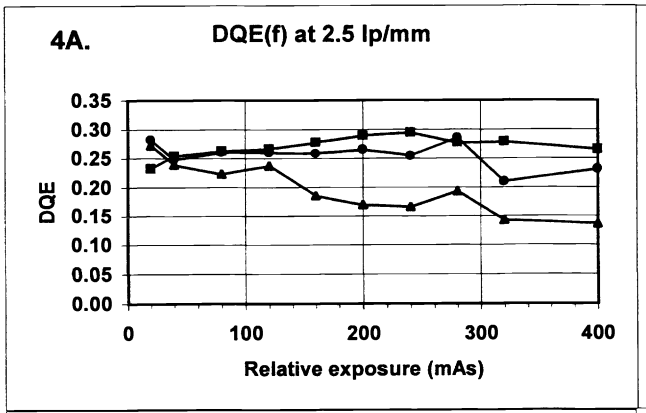

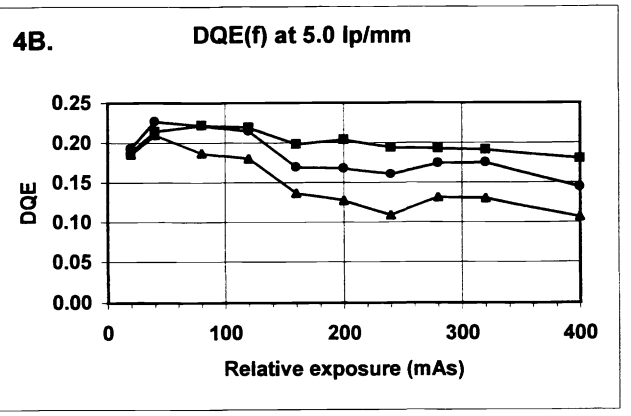

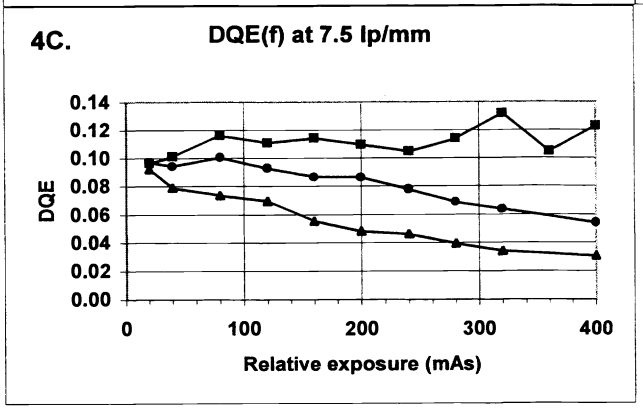

Figure 4. DQE as a function of incident exposure expressed in mAs for the flat-field correction comparisons. A. DQE at 2.5 lp/mm. B. DQE at 5.0 lp/mm. C. DQE at 7.5 lp/mm. For all plots, the square box represents the VFF technique, the circles represent FF_{320}, and triangles represent FF_{80} conventional methods.

The variable flat-field method resulted in the highest DQE, in particular for images acquired at high exposures and at high spatial frequencies. An improvement of nearly 30% in DQE(f) is demonstrated with the variable flat-field technique compared to the conventional technique, as shown in Figure 3C. A conventional flat-field method using a relatively high exposure flat-field matrix (~44 mR, corresponding to ~2600 ADU) is compared to the variable flat-field method proposed in this paper as applied to a raw image of high incident exposure. In the same example, the lower DQE results of the 80 mAs flat-field correction matrix clearly indicate the inadequacy of the low exposure flat-field acquisition to correct such a high exposure image. On the other hand, the variable flat-field matrix does not provide as much improvement in images acquired at lower exposures, most likely due to the "masking" of the stationary noise by competing random statistical noise variations. In fact, at the lowest exposures, a slight decrease in the DQE(f) is measured with the variable exposure method. This is likely due to the inclusion of noise from the flat-field correction matrix *back* into the image, caused by non-canceling signals readily manifested in the correction matrix, yet unresolved in the low exposure image by random signal variations. A small but measurable increase in noise and a corresponding decrease in the DQE thus occurs. An example is demonstrated in Figure 4 with the DQE plotted as a function of incident exposure. In 4A, a noticeably lower DQE is present for lower exposures and lower spatial frequency. The "scaling" of the flat-field matrix response, however, mitigates the noise increase by the small pixel values in the raw image. The DQE at higher spatial frequencies for the proposed method is significantly higher, attributed to the relatively noise-free estimation of the stationary noise variations on a pixel by pixel basis. While there is a definite trend to lower DQE with increased exposure for the conventional correction method at any specific spatial frequency, the variable correction method maintains a relatively constant response, as shown in Figures 4A,B and C.

Effects such as time jitter of the CCD camera, variable temporal response of the detector, pixel mismatch of the correction matrix with the raw image, or significant variations in the acquisition geometry between the flat-field acquisition procedure and the raw image to be corrected can cause poor results. The implementation of the proposed procedure is initially much more time consuming and complex, in particular during the acquisition stage of the many flat-field images required for construction of the variable flat-field matrix. It is possible that the method is much more robust in terms of the stability of the correction matrix over time. Currently, the manufacturer of the device tested here recommends a daily flat-field acquisition [8]. Other additional considerations for future investigation includes use of a uniform phantom at the detector to include the scatter distribution in the flat field procedure (the current recommended procedure) and the ability of the technique to be adapted to a non-linear detector response.

Initially it was conjectured that the best DQE response would be obtained with a flat-field correction matrix acquired at the same incident exposure as the raw image according to preliminary reports of a previous investigation [1], but the hypothesis is not supported by these results. Undoubtedly, the best possible flat-field matrix (for all but the lowest exposure images) is one obtained in the absence of statistical noise variations. This is most closely achieved by the methods described in this paper, whereby the stationary noise variations are manifested in the corresponding variations of the slope and intercept values of a linear least-squares fit obtained pixel by pixel over a range of incident exposures.

5. CONCLUSIONS

A method to create a robust flat-field correction methodology is proposed, using a digital mammography biopsy unit as the test system. When the raw image contains a wide range of incident exposures corresponding to the attenuation characteristics of an object, this method improves the elimination of fixed-point noise superimposed in the uncorrected image, particularly for higher spatial frequencies and higher incident exposures. In principle, application to clinical images for digital biopsy systems is straightforward albeit somewhat more involved initially for the acquisition of the flat-field images. Long-term usefulness has not been tested, but it is expected that this technique is more immune to temporal variations of the system response. Application of these techniques to other digital detectors appears promising, specifically to contend with non-linear responses of the exposure to pixel value in either local or global areas of the uncorrected image.

6. ACKNOWLEDGMENTS

Dr. Robert Gagne of the Center for Devices and Radiological Health assisted greatly in early discussions regarding the implementation and understanding of noise power spectrum estimates. This research was supported in part by funds from the California Breast Cancer Research Program of the University of California, Grant Number 2RB-0071.

7. REFERENCES

1. JA Seibert and JM Boone, "Image quality and radiation dose assessment of a digital mammography biopsy system", (Abstract), Radiology **193P**, 360, 1994.

2. JM Boone, TR Fewell, and RJ Jennings, "Molybdenum, rhodium, and tungsten anode spectral models using interpolating polynomials with application to mammography", Medical Physics **24**: 1863-74, 1997.

3. JM Boone, "Spectral modeling and compilation of quantum fluence in radiography and mammography", Proc SPIE **3336**, 1998 (this issue).

4. H Fujita, DY Tsai, T Itoh, K Doi, J Morishita, K Ueda, A Otsuka, "A simple method for determining the modulation transfer function in digital radiography", IEEE Transactions on Medical Imaging: **MI-11**: 34-39, 1992.

5. JC Dainty and R Shaw, *Image Science*, New York, NY, Academic Press; 1974.

6. JT Dobbins III, DL Ergun, L Rutz, DA Hinshaw, H Blume, DC Clark. "DQE(f) of four generations of computed radiography acquisition devices", Medical Physics **22**: 1581-93, 1995.

7. IA Cunningham, "Analyzing system performance", in *The expanding role of Medical Physics in Diagnostic Imaging,* GD Frey and P Sprawls, Eds. American Association of Physicists in Medicine monograph published by Advanced Medical Publishing, Madison, WI, 1997.

8. Fischer Imaging Corporation, Operator manual for the Mammovision Electronic Stereotaxy System: 77300G, P-55650-OM Issue 1, Revision D, July, 1993 and recent updates and communications for software (version 2.4).